INTERNATIONAL JOURNAL FOR NUMERICAL METHODS IN FLUIDS
Int. J. Numer. Meth. Fluids 2015; **79**:84–107
Published online 1 June 2015 in Wiley Online Library (wileyonlinelibrary.com). DOI: 10.1002/fld.4044

Numerical modeling of chlorine concentration in water storage tanks

Ramon Codina[1,2,*,†], Javier Principe[1,2], Christian Muñoz[3] and Joan Baiges[1]

[1]*Centre Internacional de Mètodes Numèrics en Enginyeria, Jordi Girona 1-3, Campus Nord UPC, Edifici C1, 08034 Barcelona, Spain*
[2]*Universitat Politècnica de Catalunya, Jordi Girona 1-3, Edifici C1, 08034 Barcelona, Spain*
[3]*Universidad Tecnológica Metropolitana, Departamento de Mecánica Av. José Pedro Alessandri 1242, Ñuñoa, Santiago, Chile*

SUMMARY

In this paper, we describe a numerical model to simulate the evolution in time of the hydrodynamics of water storage tanks, with particular emphasis on the time evolution of chlorine concentration. The mathematical model contains several ingredients particularly designed for this problem, namely, a boundary condition to model falling jets on free surfaces, an arbitrary Lagrangian–Eulerian formulation to account for the motion of the free surface because of demand and supply of water, and a coupling of the hydrodynamics with a convection–diffusion–reaction equation modeling the time evolution of chlorine. From the numerical point of view, the equations resulting from the mathematical model are approximated using a finite element formulation, with linear continuous interpolations on tetrahedra for all the unknowns. To make it possible, and also to be able to deal with convection-dominated flows, a stabilized formulation is used. In order to capture the sharp gradients present in the chlorine concentration, particularly near the injection zone, a discontinuity capturing technique is employed. Copyright © 2015 John Wiley & Sons, Ltd.

Received 1 October 2014; Accepted 19 April 2015

KEY WORDS: water storage tanks; chlorination; stabilized formulations; arbitrary Lagrangian-Eulerian formulations; jet boundary conditions

1. INTRODUCTION

To minimize short-circuit and dead zones and to guarantee treatment process efficiency are problems commonly encountered in the design and optimization of water storage tanks. These tanks are the final phase of drinking water treatment plants; the whole process includes mixing and contact tanks, reaction and phase separation tanks, and storage and distribution tanks [1].

The objective of water storage tanks is twofold, namely, to equalize demand fluctuations (pumping requirements and operating pressures) and to provide storage for fire fighting and emergencies [2]. Many efforts have been performed to understand the different phenomena that occur inside these tanks. From the hydraulic point of view, there are two types of ideal flow within reactors, the so-called plug (or piston) and mixed (or stirred) flows [3]. Examples of the first one are the contact tanks, where contact between water and reactive substance (for instance chlorine) must be maximized. To achieve this objective, it is necessary to prevent that freshly inflow be remixed with the fluid inside the tank [1]. Existence of baffles is the main characteristic of contact tanks; they redirect the flow path in a narrow long path, and as a result, the residence times of all the particles inside the tank are the same [3]. In the second group, there are generally the storage tanks, where the mix

*Correspondence to: Ramon Codina, Dept. de Resistència de Materials i Estructures a l'Enginyeria, Universitat Politècnica de Catalunya,Jordi Girona 1-3, Edifici C1, 08034 Barcelona, Spain.
†E-mail: ramon.codina@upc.edu

of freshly inflow with the content of the tank is preferred. Water quality in storage tanks was not considered in early times for the design, but nowadays, it is an important objective to satisfy water regulations, because presence of total mix in the tank keeps the bulk water quality.

Real flows inside tanks are difficult to categorize because of complex geometries and inlet–outlet configurations, where presence of stationary and recirculation zones are common, and consequently, poor mixing and long residence times occur, implying long water age.

Nowadays, chlorine is the most common disinfectant used in drinking water treatment plants. As a non-selective oxidant, chlorine in the water tanks reacts with both organic and inorganic chemical species, leading to the formation of disinfection by-products [4], as total trihalomethanes [5]. Bad hydraulic performance of tanks, as the presence of short-circuit and dead zones, impacts in the effectiveness of the chlorine disinfection. The main consequence of chlorine decay (because of its reactions with species) is that for long residence time of fluid particles, the amount of chlorine diminishes (in fact exponentially), and poor concentration of disinfectant stimulates the bacterial regrowth. As the general regulations require that minimum levels of chlorine must be maintained in the entry to the distribution system [6], it is often necessary a second rechlorination in storage tanks [7].

Modeling the performance of real drinking water storage tanks consists of two stages. On the one hand, it is necessary to simulate the hydrodynamic behavior inside the tank according to the inlet–outlet configuration and pumping requirements. Some authors have mentioned the need of considering the variable water level in response to variable inlet–outlet flow, so that the flows are never steady [7]. On the other hand, it is necessary to simulate the chlorine transport (and decay) according to the velocity field. Simplified mathematical models of the whole process can be found in the literature [1]. For example, in the so-called black box model, an ideal behavior inside the tank (total mix) and an uniform concentration of chlorine are assumed [2]. In the opaque box model, the domain is split in zones with simplified different behavior (boundary volume zone, zone of fixed stagnant volume, region of variable mixed volume, recirculation zones, etc.) and is assembled in a compartment circuit to represent in more detail the complex hydrodynamic behavior inside the tank. Examples of opaque box models are the multichannel reactor model [7] and the linear compartment model [8]. Obviously, another way to approach the problem is experimentally using scale models. Important advances have been achieved using three-dimensional laser-induced fluorescence [9] and digital image techniques [10] in tracer studies.

Analytical models of chlorine concentration decay are based on mass conservation. The unsteady advection–diffusion–reaction (ADR) equation is the most used in computational modeling of decay [1, 11]. In particular, the simplest and most used model is to consider only a linear reaction term in the ADR equation, where the reaction coefficient is the decay constant of chlorine [12]. This is the so-called first-order model. The decay constant is usually calculated by means of regression lines with experimental data using least square methods. It is well known that it depends on temperature variations and initial concentration of chlorine, and also on the concentration of organics and the reactivity of these in water [13]. Several models of decay have been presented in order to capture all these phenomena, such as the second-order model [14], the parallel first-order model [15], and the parallel second-order model [4]. It is assumed in general that chlorine reacts in two ways in water. There is an initial phase of rapid consumption (fast reaction) and a second of slow consumption (long-term reaction). The different combinations of first and second orders of the decay of these two phases give rise to the parallel models.

Computational modeling nowadays is widely used in studies of water treatment plants, for instance, in chlorine contact tanks [16–21], settling tanks [22], clarification basins [23], distribution system [24], bacterial inactivation [25], and storage tanks [7, 26–28]. Computational models are also used for the chlorine concentration decay [1, 11].

Jets are the only mechanism to achieve mixing in storage tanks because these work without any active devices, such as turbines or impellers [29]. When a jet reaches the sides of the tank, it reverses its direction, stimulating the remix of the fluid inside the tank with new freshly inflow water. Adding to this, the complexities of the geometries of tanks and the formation of recirculation zones and secondary flows are common, so the flow is dominated by three-dimensional large-scale structures,

DOI: 10.1002/fld

as in contact tanks [20]. Early efforts to capture these phenomena were to use the Reynolds-averaged models of the Navier–Stokes equations (RANS) as in [21], where the popular k-ε model was employed to calculate the turbulent eddy viscosity and the water surface was kept constant. Other approaches were to use depth-integrated equations instead of the three-dimensional Navier–Stokes equations, as in [18, 30]. In these references, the authors compared different RANS turbulence models, as the mixing length and the k-ε model, and Smagorinsky's subgrid-scale eddy viscosity model (SGS) to approximate the Reynolds stress in a large eddy simulation (LES). They concluded that the mixing length model was not adequate to capture horizontal re-circulations, which the k-ε model overestimated diffusive effects in the flow, and finally that Smagorinsky's model underestimated peak concentrations of chlorine compared with measurements. Other authors have concluded the same [16]. Nowadays, LES in this context has put aside the traditional RANS models [20, 24], although some authors have used unsteady RANS to study jet mixing in storage tanks [26]. The approach we have adopted in this paper is not to use any turbulence model, but to rely on the dissipation of the numerical formulation to model the subgrid scales of turbulence. This strategy is commonly known as implicit large eddy simulation.

In this work, we present a model to simulate the behavior of real drinking-water tanks with several particular features. First, we take into account the variability of the volume of water because of its demand and supply, which are supposed to be known at all times. Second, we will also propose a model to approximate the effect caused by the jets of fresh water impinging the free surface of the storage tank. Finally, we also consider the injection of chlorine through little jets, its transport, diffusion, and decay.

Section 2 presents the mathematical model. Concerning the variability of the volume of water, the demand–supply curves we will use are based on a 24-h operation of the plant, the data we have available for the numerical simulations to be presented of real drinking-water storage tanks close to the city of Barcelona. We start with a given level of the water-free surface at a certain time, and calculate the instantaneous level of the free surface from the incoming and outcoming flow rates given by the demand–supply curves. To model mathematically the process, the incompressible Navier–Stokes equations are written using a particular arbitrary Lagrangian–Eulerian (ALE) formulation (see e.g., [31]). Referring to the treatment of jets, this is required in a very common case where water is supplied to the tank through jets that hit the water-free surface. We propose to model this from the knowledge of the jet velocity exit and geometry, assuming a parabolic free falling and computing its spreading using the self-similarity of turbulent jets as hypothesis [32, 33]. The velocities that reach the tank-free surface are then used as boundary conditions. Finally, for the chlorine concentration model, we use the first-order model described earlier.

The numerical approximation of the mathematical model is described in Section 3. It is based on a finite element method implemented in an in-house finite element software package. This formulation in turn is based on a nodal-based structure that makes it more efficient than standard codes with an element-based data structure [34]. In order to overcome instabilities that arise because of the coupling of velocity and pressure and to be able to deal with convection-dominated problems, an orthogonal subgrid-scale stabilization is used [35]. A predictor–corrector scheme based on fractional step methods is used to segregate the velocity–pressure coupling [36]. The approximation of the equation for the chlorine concentration is also based on a stabilized finite element method. However, in this case it is also necessary to use a shock-capturing method to deal with the sharp gradients that appear close to the chlorine injection jet.

Numerical simulations are presented in Section 4. We first present some simple tests to validate some of the new approximations (physical and numerical) proposed in this paper. Then we present two numerical simulations of real water storage tanks. From these, one can evaluate the potential of the model we propose to extract conclusions about the behavior of the tank of physical and technological interest. Studies of these tanks are generally centered in finding the optimum inlet–outlet configuration of the flow to preserve the complete mix in its operation period. For example, preliminary conclusions in computational modeling of steady-state situations are that a side wall inlet, below the free surface, is better than the top water level inlets in geometries where the outflow is placed in the opposite side of the inlet in rectangular tanks [7]. Similar conclusions in transient experimental scale model studies were obtained in [10]. Other scale model studies relate the amount

DOI: 10.1002/fld

of inlet with the mixing fastness [9]. In one of the simulations presented, the tank studied is of cylindrical type with an upward inlet jet in the center. We show that our simulation captures the 'donut'-type dead zone presented in scale models [9]. Furthermore, this tank has several columns inside. Effects of columns in mixing of storage tanks have been studied in scale model tracer studies in [10, 17]. Preliminary conclusions of these works are that wake areas behind columns behave as emitters of tracer into the bulk of the flow, favoring the local mixing but slowing the velocity field. In order to measure the hydraulic efficiency of the tank, there are several experimental indexes [37], the most common of which is the residence time distribution (RTD) of a tracer (conservative substance) transported inside the tank. RTD curves are obtained normalizing the concentration of the tracer measured in the outflow by the initial average concentration in a steady-state flow. As tanks studied in this work operate in unsteady state, we use the fraction of the tank volume occupied by the dead region [25, 38] as hydraulic index.

The paper is closed in Section 5 with some final conclusions and remarks.

2. MATHEMATICAL MODEL

This section is devoted to the description of the mathematical model needed to simulate the operation of a storage tank in a certain time period. The model includes the flow problem, described by the incompressible Navier–Stokes equations, and the balance equation for the chlorine concentration, both with appropriate boundary conditions.

A possible geometrical configuration of the storage tanks to be considered is depicted in Figure 1. It consists of a round tank, with columns supporting the lid (not shown) and with two types of inflows, namely, one below the water-free surface (in this case emanating from a pipe that arises from the ground) and another above it. The latter gives rise to a free-falling jet. There might be different outlets in the tank, usually through holes with small diameters compared with the tank size.

2.1. *Hydrodynamical model and free surface motion*

2.1.1. Incompressible Navier–Stokes equations. Let $\Omega(t)$ be the domain occupied by the water at a certain time $t \in [0, T]$, where T is the duration of the time interval to be analyzed. This domain is time dependent because of the possible mismatch between outflow–inflow flow rates given by the demand–supply curves, as described later. We assume throughout that $\Omega(t)$ is three-dimensional, with boundary $\Gamma(t) = \partial\Omega(t)$. At each point of $\Gamma(t)$, $\boldsymbol{n}$ will be the unit outward normal and $\boldsymbol{m}_i, i = 1, 2$, the two tangent vectors, being $\boldsymbol{n}, \boldsymbol{m}_1, \boldsymbol{m}_2$ an orthonormal system.

Let $\boldsymbol{u} : \Omega(t) \times [0, T] \longrightarrow \mathbb{R}^3$ be the water velocity at each point and time instant $(\boldsymbol{x}, t) \in \Omega(t) \times [0, T]$, and $p : \Omega(t) \times [0, T] \longrightarrow \mathbb{R}$ the kinematic pressure. We consider that $\boldsymbol{u}$ and p are unaffected by the concentration of substances in the water tank, in particular by chlorine, that is, it is

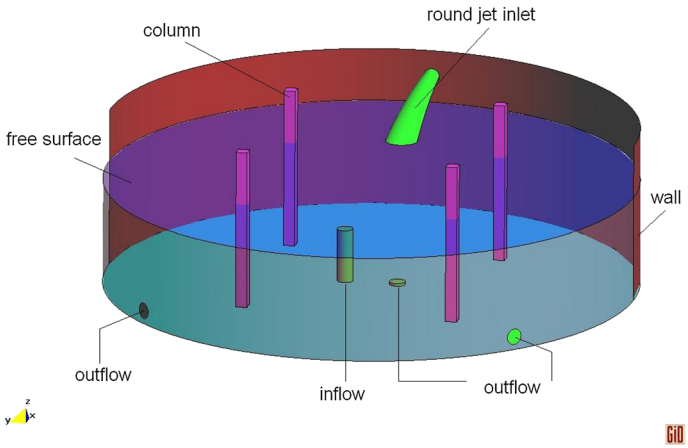

Figure 1. A generic example of a ground storage tank.

DOI: 10.1002/fld

assumed to be a passive scalar. Therefore, $\boldsymbol{u}$ and p are solution of the incompressible Navier–Stokes equations, given by

$$\partial_t \boldsymbol{u} - 2\nu\nabla\cdot\nabla^s\boldsymbol{u} + \boldsymbol{u}\cdot\nabla\boldsymbol{u} + \nabla p = \boldsymbol{f} \quad \text{in}\,\Omega(t)\times(0,T) \tag{1}$$

$$\nabla\cdot\boldsymbol{u} = 0 \quad \text{in}\,\Omega(t)\times(0,T) \tag{2}$$

where ν is the kinematic viscosity (the dynamical viscosity divided by density), ∇^s is the symmetrical gradient, and $\boldsymbol{f}$ is the force vector. For the exposition, we will consider only gravity forces, and therefore $\boldsymbol{f}$ could be taken as zero and the hydrostatic pressure added to p. This will allow us to prescribe zero traction boundary conditions at free outlets, whereas otherwise the hydrostatic pressure should be prescribed.

Equations (1) and (2) must be supplied with an initial condition of the form $\boldsymbol{u} = \boldsymbol{u}^0$ in $\Omega(0), t = 0$, and suitable boundary conditions on $\Gamma(t), t \in [0,T]$. The particular features of the problem described rely precisely on these boundary conditions, which will be discussed in detail later.

Even though we will not consider thermal coupling, which could be incorporated through Boussinesq's assumption, in some studies, water stratification due to density variations caused by temperature is taken into account [9].

2.1.2. Demand–supply curves and free surface motion. Variability of the water volume inside tanks, for example, in a complete 1-day operation of the plant, is due to the mismatch between inflows and outflows. The so-called demand–supply curves determine the time evolution of the outflow and inflow flow rates, respectively.

From the demand–supply curves we can determine the following:

- The time variation of the position of the free surface.
- The velocity boundary conditions.

We will assume that the free surface can be modeled as a perfectly flat surface. This is an approximation in two senses. On the one hand, if there are water jets hitting the free surface, there will be local dynamics around the impact zone that will not be taken into account. On the other hand, there might be surface waves produced by the water volume variation. This last effect is negligible in the problem we consider.

Under the assumption described, the position of the free surface can be easily determined from the net flow rate and the geometry of the tank. The net flow rate determines the volume variation and, from this, the variation of the free-surface height.

The velocity boundary condition requires to assume a certain velocity profile to produce the inflow and outflow flow rates in the inlet and outlet pipes; we will assume this profile to be parabolic in all cases.

Figure 2 (left) shows a demand–supply curve along a certain operation period in one of the examples that we have analyzed. From these curves, the position of the free surface can be easily computed for a given geometry as follows. Suppose that a given time t, the area of the free surface

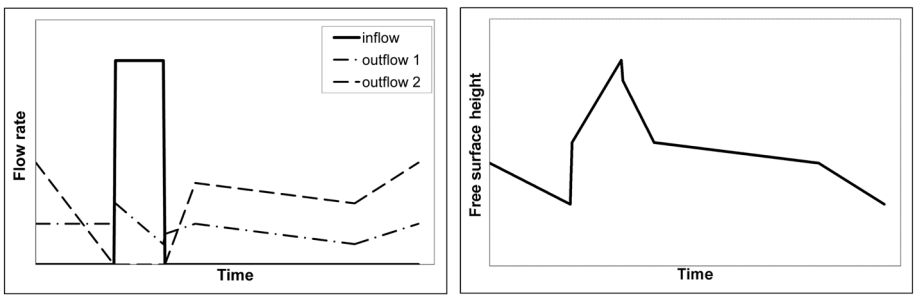

Figure 2. Demand flow rate curves in a tank with one inflow and two outflows (left) and free surface height curve of this tank obtained from the demand curves (right).

DOI: 10.1002/fld

is $A(t)$, the inflow flow rate $Q_{\text{in}}(t)$ (possibly from different inlets), and the outflow flow rate $Q_{\text{out}}(t)$ (possibly from different outlets). Then, $H(t)$ is computed from the time integration of

$$\frac{\mathrm{d}}{\mathrm{d}t}H(t) = \frac{1}{A(t)}\left(Q_{\text{in}}(t) - Q_{\text{out}}(t)\right)$$

This integration can be performed numerically.

For the example of Figure 2 (left), the evolution of the height $H(t)$ of the free surface is shown in Figure 2 (right).

2.1.3. A particular arbitrary Lagangrian–Eulerian formulation. Because of the time variation of the free-surface height, the domain $\Omega(t)$ where the problem is posed is time dependent. To deal with this time evolution, we will use a simplified Arbitrary Lagangrian–Eulerian (ALE) formulation.

If $H(t)$ is the free surface height computed as described earlier, the velocity of this free surface is given by

$$\boldsymbol{u}^{\text{f}}(t) = \frac{\mathrm{d}}{\mathrm{d}t}H(t)\boldsymbol{e}_3 \tag{3}$$

where $\boldsymbol{e}_3$ is the unit vector in the vertical direction. From the free surface velocity $\boldsymbol{u}^{\text{f}}(t)$, we may define a domain velocity $\boldsymbol{u}^{\text{d}}(\boldsymbol{x},t)$, which in the finite element approximation described later will correspond to the velocity of the nodes of the finite element mesh. Very often, this velocity field is obtained by solving an equation of Laplace type in the whole domain Ω. In [39], there is an example of the change in volume in a simple discharge of a tank using this procedure. Here, however, we will use a simpler specifically designed procedure.

We have to differentiate two situations, namely, the case in which the free surface is above the inlet (Figure 3 left) and the one in which the inlet is above the free surface (Figure 3 right). We will assume that there are no other operational situations in the tank, that is to say, submerged inlets never get above the free surface. This is the common situation in real water storage tanks.

In both cases, we have a region limited by the planes $x_3 = H_0$ and $x_3 = H(t)$, where x_3 is the vertical coordinate and H_0 is a height that we take just above the inlet in the first case and just above the highest outlet in the second. In this region $\Omega_H(t)$, we compute the velocity $\boldsymbol{u}^{\text{d}}(\boldsymbol{x},t)$ by solving the problem

$$\Delta\boldsymbol{u}^{\text{d}}(\boldsymbol{x},t) = \boldsymbol{0} \qquad \text{in } \Omega_H(t) \tag{4}$$

$$\boldsymbol{u}^{\text{d}}(\boldsymbol{x},t) = \boldsymbol{u}^{\text{f}}(t) \qquad \text{at } x_3 = H(t) \tag{5}$$

$$\boldsymbol{u}^{\text{d}}(\boldsymbol{x},t) = \boldsymbol{0} \qquad \text{at } x_3 = H_0 \tag{6}$$

$$\boldsymbol{n}\cdot\boldsymbol{u}^{\text{d}}(\boldsymbol{x},t) = 0, \quad \boldsymbol{m}_i\cdot(\boldsymbol{n}\cdot\nabla\boldsymbol{u}^{\text{d}}(\boldsymbol{x},t)) = 0,\ i = 1,2, \qquad \text{on the rest of } \partial\Omega_H \tag{7}$$

Note that if $\Omega_H(t)$ is a cylindrical domain, $\boldsymbol{u}^{\text{d}}(\boldsymbol{x},t)$ will vary linearly from $\boldsymbol{0}$ at $x_3 = H_0$ to $\boldsymbol{u}^{\text{f}}(t)$ at $x_3 = H(t)$. This is the situation in the numerical simulations to be presented.

Once the domain velocity $\boldsymbol{u}^{\text{d}}(\boldsymbol{x},t)$ has been computed, we may rewrite Equation (1) in ALE form as

$$\partial_t\boldsymbol{u} - 2\nu\nabla\cdot\nabla^s\boldsymbol{u} + \boldsymbol{c}\cdot\nabla\boldsymbol{u} + \nabla p = \boldsymbol{f} \tag{8}$$

where the convective velocity is $\boldsymbol{c} = \boldsymbol{u} - \boldsymbol{u}^{\text{d}}$.

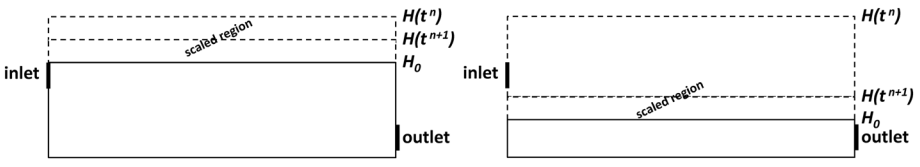

Figure 3. Type of scaling to account for movement of the free surface: inlet below the free surface (left) and inlet above the free surface (right).

DOI: 10.1002/fld

2.1.4. Initial and boundary conditions. Problems (1) and (2) need to be supplied with initial and boundary conditions. Concerning the latter, there are different types of them to be considered. The simplest cases are described later, leaving for the next subsection the case of a free falling jet.

Initial conditions. If the demand–supply curves were considered periodical, instead of considering initial conditions at $t = 0$, we could consider periodical conditions between $t = 0$ and the operational period $t = T$. However, this is not the case we will consider, and we will start the analysis from a given velocity field $\boldsymbol{u}^0(\boldsymbol{x})$ at $t = 0$.

In order to obtain a velocity field that satisfies the continuity equation (2) and the boundary conditions described later, we obtain $\boldsymbol{u}^0(\boldsymbol{x})$ by solving an instantaneous Stokes problem at $t = 0$ with these boundary conditions.

Boundary conditions on solid walls. On the bottom of the tank, we prescribe the non-slip condition $\boldsymbol{u} = \boldsymbol{0}$. On the lateral surfaces, the fluid needs to slip because of the motion of the free surface. We then prescribe the non-penetration condition $\boldsymbol{n} \cdot \boldsymbol{u} = 0$, associated with the prescription of zero tangential stresses. Tangential stresses based on wall laws could also be prescribed, but we have not considered them in this work.

Boundary conditions at inlets and outlets. From the demand and supply curves, we know the inflow and outflow flow rates at inlets and outlets, respectively. If $q(t)$ is the flow rate at any of these and a is its area, the mean of the velocity to be prescribed is $q(t)/a$. In the examples, we have considered inlets and outlets as round pipes, and we have prescribed a parabolic velocity profile pointing in the direction of pipe, normal to the tank.

At the numerical level, and in order to avoid possible mismatch of inflow, outflow, and free surface motion, it is convenient to leave at least one outlet free, that is to say, to prescribe zero traction there (or the natural Neumann boundary condition associated to (1)).

Boundary conditions on the free surface. If there is a jet of water that impacts the free surface, the velocity prescribed is obtained as described later. At all other points, we prescribe the normal velocity to $\boldsymbol{n} \cdot \boldsymbol{u}^{\mathrm{f}}(t)$ given by (3) and leave free the tangential component, so that we will in fact prescribe the tangential stress to be zero.

2.1.5. Variational problem. According to the previous discussion, the boundary conditions to be considered will be of the following form:

$$\begin{aligned} \boldsymbol{u} &= \bar{\boldsymbol{u}} && \text{on } \Gamma_D \\ \boldsymbol{n} \cdot \boldsymbol{u} = \bar{u}_n, \quad \boldsymbol{m}_i \cdot (\boldsymbol{n} \cdot \boldsymbol{\sigma}) &= 0,\ i = 1, 2, && \text{on } \Gamma_M \\ \boldsymbol{n} \cdot \boldsymbol{\sigma} &= \boldsymbol{0} && \text{on } \Gamma_N \end{aligned}$$

where $\Gamma = \Gamma_D \cup \Gamma_M \cup \Gamma_N$, $\bar{\boldsymbol{u}}$ is a given velocity field, $\bar{u}_n$ a given normal velocity, and $\boldsymbol{\sigma} = -p\boldsymbol{I} + 2\nu\nabla^s\boldsymbol{u}$ is the Cauchy stress tensor (divided by the density). Γ_D is the union of the inlet, the outlet with prescribed velocity, the jet on the free surface (if it exists) and the bottom of the tank, whereas, Γ_M is the union of the rest of the free surface and the lateral surfaces of the tank. Γ_N is the part of the boundary where the velocity is left free, which in our case corresponds to one of the outlets, as explained earlier.

Let us define the functional spaces

$$V := \left\{ \boldsymbol{v} \in H^1(\Omega)^3 \mid \boldsymbol{v} = \bar{\boldsymbol{u}} \text{ on } \Gamma_D, \boldsymbol{n} \cdot \boldsymbol{v} = \bar{u}_n \text{ on } \Gamma_M \right\}$$

$$V_0 := \left\{ \boldsymbol{v} \in H^1(\Omega)^3 \mid \boldsymbol{v} = \boldsymbol{0} \text{ on } \Gamma_D, \boldsymbol{n} \cdot \boldsymbol{v} = 0 \text{ on } \Gamma_M \right\}$$

as well as $Q = L^2(\Omega)$. As usual, $H^1(\Omega)$ denotes the space of functions with derivatives in $L^2(\Omega)$. The inner product in this space is denoted by $(\cdot, \cdot)$, whereas in general, $\langle \cdot, \cdot \rangle$ denotes the integral of the product of two functions.

DOI: 10.1002/fld

With the notation introduced, the weak form of the problem consists of finding a velocity $\boldsymbol{u} : [0,T] \longrightarrow V$ satisfying the initial condition and a pressure $p : [0,T] \longrightarrow Q$ such that

$$(\partial_t \boldsymbol{u}, \boldsymbol{v}) + \langle (\boldsymbol{u} - \boldsymbol{u}^{\mathrm{d}}) \cdot \nabla \boldsymbol{u}, \boldsymbol{v} \rangle + 2\nu \, (\nabla^s \boldsymbol{u}, \nabla^s \boldsymbol{v}) - (p, \nabla \cdot \boldsymbol{v}) = \langle \boldsymbol{f}, \boldsymbol{v} \rangle \tag{9}$$

$$(q, \nabla \cdot \boldsymbol{u}) = 0 \tag{10}$$

for all $\boldsymbol{v} \in V_0$ and $q \in Q$.

2.2. *Free falling round jet model*

Certain tanks are fed in a waterfall manner (free falling), that is to say, one or more water jets are thrown out over the free surface of the water inside the tank [10]. In other tanks, inlets are placed below the free surface of water, but may become located above this free surface if the tank is emptied. To model this situation while avoiding to simulate numerically these jets, we propose to use the semi-empirical velocity profiles obtained in theoretical and experimental studies of developed jets issuing in a quiescent medium. We are interested in the profile of radial and axial velocity (in the direction of the motion) and the spread of the jet.

We will start explaining how to model numerically a straight water jet entering air using empirical information. In particular, we will assume that the jet is a round one and explain how to approximate the radius evolution and the velocity profile inside the jet. Assuming that the jet leaves horizontally, we will compose the dynamics described with the free falling of the jet until it touches the free surface. This will allow us to obtain the velocity (magnitude and direction) of the water particles that reach the tank, and which we will prescribe as boundary conditions. The simplification of considering a constant radius of the jet and a uniform velocity will also be described. In fact, in the numerical simulations, we will present that we have observed that this is a good approximation.

2.2.1. Straight water jets in air. Let us consider a jet from a circular hole of radius R_0 and uniform velocity U_0. To fix ideas, we assume that the jet is horizontal and remains straight, that is, gravitational effects are neglected for the moment. Let L be the length coordinate along the jet axis and r the radial distance along this axis. We assume that the jet remains round, with diameter $R(L)$ and with an axial velocity profile $U(r, L)$. The objective is to determine $R(L)$ and $U(r, L)$ from experimental results.

The jet radius $R(t)$ grows because of pressure release and air entrapment caused by instabilities on the jet surface. It depends on the geometry of the problem, the velocity U_0, and the physical properties of water and air, including water surface tension. Different models of more or less complexity can be found, for example, in [40–43]. Here, we will use a very simple model, which can be found, for example, in [44–46]. The outer surface of the jet is assumed to grow linearly with the distance, and therefore

$$R(L) = CL + R_0 \tag{11}$$

where C is a constant. For example, the value $C = 0.005$ is suggested in [46] for high Reynolds numbers, as those encountered in water jets feeding tanks.

It remains now to obtain the velocity profile $U(r, L)$. Let $M(r, L)$ be the momentum. Neglecting the density of the air bubbles, it will be given by

$$M(r, L) = \rho \alpha(r, L) U(r, L) \tag{12}$$

where ρ is the water density and $\alpha(r, L)$ is the water volume fraction. Note that $\alpha(0, 0) = 1$. After the inlet, the jet displays a zone of flow establishment of length between $10R_0$ and $20R_0$ where α varies significantly with r, being close to 1 in the core of the jet. In the zone of fully developed jet, we may assume that mixing with air is uniform in the whole section, so that $\alpha(r, L) = \alpha(0, L)$. This function $\alpha(0, L)$ is known experimentally. In [47], it is shown that it decreases rapidly with L, being approximately $\alpha(0, 40R_0) \approx 0.2, \alpha(0, 200R_0) \approx 0.05, \alpha(0, 400R_0) \approx 0.02$. We will determine it by imposing conservation of the flow rate.

DOI: 10.1002/fld

We may now proceed to compute $U(r, L)$. For that, we need to use the profile $M(r, L)$, which from experimental results can be shown to match the curve [45]:

$$M(r, L) = M(0, L)\left[1 - \left(\frac{r}{R}\right)^{3/2}\right]^3 \tag{13}$$

From the continuity equation, we have that the integral of $M(r, 0)$ over the inlet section $L = 0$ should be equal to the integral over any other section, that is to say,

$$\rho U_0 \pi R_0^2 = 2\pi M(0, L) \int_0^R \left[1 - \left(\frac{r}{R}\right)^{3/2}\right]^3 r \, \mathrm{d}r,$$

from where [45]

$$M(0, L) = 5.62\, \rho U_0 \frac{R_0^2}{R^2} \tag{14}$$

Using (14) in (13) and the definition (12), we finally get:

$$U(r, L) = 5.62\, U_0 \frac{R_0^2}{\alpha\, R^2}\left[1 - \left(\frac{r}{R}\right)^{3/2}\right]^3 \tag{15}$$

where $R = R(L)$ is given by (11) and α is known experimentally or can be determined from the conservation of the water flow rate.

2.2.2. Free falling of water jets. In the previous development, we have assumed that the jet is horizontal. However, it will fall because of gravity and impact the water-free surface of the tank. A schematic of the situation is depicted in Figure 4.

The vertical and the horizontal motions are coupled, because the vertical acceleration will lead to a velocity increase that depends nonlinearly on the radius of the jet, which in turn depends on the length run by the jet particles. To simplify the problem, we will consider that the horizontal and vertical motions can be uncoupled, the former with the kinematics described previously and the latter with the kinematics of a free falling.

Once we know the motion of all water particles in the inlet jet, we may compute the point and the velocity at which these particles will impact the free surface. Then, we may prescribe this velocity as a Dirichlet boundary condition at the point of impact. Let us see how to compute the impact point and velocity.

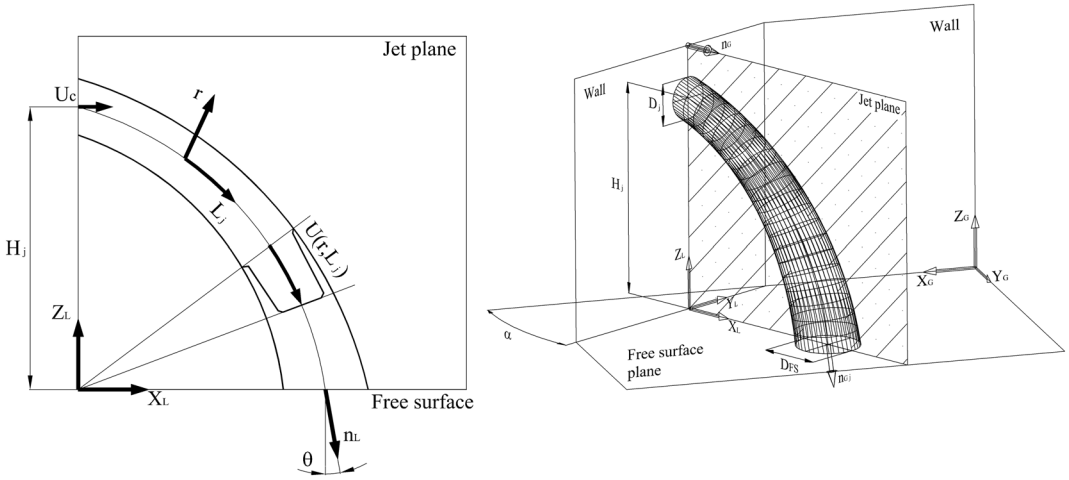

Figure 4. Free falling of a jet. Left: plane section and right: perspective.

DOI: 10.1002/fld

For each particle in the jet, let $z(t)$ be the vertical coordinate measured from the tank-free surface at time t. Assuming the vertical motion corresponds to free falling, it will be given by

$$z(t) = z_0 - \frac{1}{2}gt^2 \tag{16}$$

where $z_0 = z(0)$. The impact with the free surface will take place at $T_\mathrm{f} = T_\mathrm{f}(z_0) = \sqrt{2z_0/g}$. If r_0 is the radial coordinate of the particle at the inlet, the horizontal distance $L(r_0, z_0, t)$ run after a time t can be obtained by solving

$$\frac{\mathrm{d}L}{\mathrm{d}t} = U(r, L), \quad L(r_0, z_0, 0) = 0 \tag{17}$$

where, according to (11), $r = CL + r_0$. The horizontal distance run by the particle will be $L_\mathrm{f} = L(T_\mathrm{f})$, with $L(t)$ computed by solving (17). With this, we could compute the shape of the intersection of the falling jet with the free surface exactly. However, this would involve discretizing the section of the inlet jet and integrating (17) for all discretization points. Rather than this, we compute the shape of the intersection in a simplified manner.

Assume that $R(L) \approx R_0$ and $U(r, L) \approx U_0$, that is to say, the jet maintains its radius and the velocity is uniform, equal to the inlet velocity. With these simplifications, we have that $L_\mathrm{f} = U_0 T_\mathrm{f}$, which allows us to compute the coordinates of the jet impacting the free surface, and the velocity at the center of the jet, which is

$$\boldsymbol{u}_0^{\mathrm{jet}} = (U_0, -gT_\mathrm{f}) \tag{18}$$

If the cross-section of the jet remains a circle of radius R, the intersection with the free surface will be an ellipse, of semi-axis R in the cross-wind direction and semi-axis $R/\cos(\theta)$ in the streamline direction (see Figure 4, left), with $\theta = \arctan(U_0/gT_\mathrm{f})$. This completely defines the shape of the intersection of the jet with the free surface, say $\Gamma_{\mathrm{jet}} \subset \Gamma_D$.

Now let $\hat{\boldsymbol{u}} = \boldsymbol{u}_0^{\mathrm{jet}}/|\boldsymbol{u}_0^{\mathrm{jet}}|$. The boundary condition on Γ_{jet} to be prescribed is

$$\boldsymbol{u}^{\mathrm{jet}} = U(r, L_\mathrm{f})\hat{\boldsymbol{u}} \tag{19}$$

where $U(r, L)$ is given by (15), with α determined from the condition that

$$\pi R^2 U_0 = \int_{\Gamma_{\mathrm{jet}}} U(r, L)\cos(\theta)$$

Alternatively to prescribing (19) with the velocity profile $U(r, L_\mathrm{f})$, we can consider a simplification, which consists in taking a constant velocity profile, so that

$$\boldsymbol{u}^{\mathrm{jet}} = U_0\hat{\boldsymbol{u}} \tag{20}$$

Note that neither in (19) nor in (20), we have considered the vertical component of the velocity in its norm, but only in its direction given by $\hat{\boldsymbol{u}}$. Increasing the velocity norm would amount to reducing the area of the intersection of the jet with the free surface, thus requiring a finer discretizaion when approximating the equations numerically.

From the simulations run, we have observed that similar results are obtained using either (19) or (20). In Section 4, we will show this quantitatively in a simple example. The simulations of water storage tanks in this section have been obtained using (20).

2.3. Chlorine decay model

2.3.1. Governing equation. The time and space evolution of the chorine concentration C is modeled using the ADR equation [1, 11]:

$$\partial_t C + \boldsymbol{c} \cdot \nabla C - \nabla \cdot (\kappa_{\mathrm{eff}} \nabla C) + r\,(C) = 0 \qquad \text{in } \Omega(t) \times (0, T) \tag{21}$$

DOI: 10.1002/fld

where $\boldsymbol{c}$ is the advection velocity to be specified later, κ_{eff} the effective diffusion coefficient, and $r(C)$ the reactive term.

Diffusion coefficient. The effective diffusion κ_{eff} is often taken as the sum of the chorine molecular diffusion κ_{mol} and a turbulent diffusion κ_{tur}. The latter in turn is taken as a turbulent Prandtl number associated with the chlorine concentration (in general, a number close to one) multiplying the turbulent kinetic viscosity associated with the turbulence model being used. However, we will not include any turbulence model in our approach, Because we rely only in the numerical formulation to be described later to model turbulence effects [35, 48, 49]. Therefore, we shall take $\kappa_{\text{eff}} = \kappa_{\text{mol}}$.

Reactive term. The reactive term $r(C)$ models the point-wise decay of chlorine concentration. The simplest and most widely used are power-law models of the form

$$r(C) = k\, C^n \tag{22}$$

where k is the bulk reaction coefficient and n the reaction order. When $n = 1$, one obtains the so-called *first-order* decay model and k the first-order decay constant of chlorine [12]. This constant is commonly calculated by linear regression from experimental data using least square methods. These data are measurements of chlorine concentration decay in glass bottle samples (where water is motionless), that is, values reported in literature are independent of the advection flow and the diffusion within the tanks. It is well known that the value of k depends on temperature variations and initial concentration of chlorine, and also on the concentration of organics and the reactivity of these in water [13]. This is why several models of chlorine decay have been proposed in order to capture all these phenomena, such as the second-order model [14], the parallel first-order model [15], and the parallel second-order model [4]. It is assumed in general that chlorine reacts in two ways in water. First, there is an initial phase of rapid consumption (fast reaction) and then a second slow consumption phase (long-term reaction). The different combinations of first and second order phases of decay give rise to the different models available in the literature.

In this work, we shall restrict ourselves to the simplest first-order model. In particular, in the numerical simulations we have used as physical constants in SI units, $\kappa_{\text{mol}} = 10^{-9}\left[\text{m}^2\text{s}^{-1}\right]$ and $k = 10^{-5}\left[\text{s}^{-1}\right]$, suggested in [11].

Advection velocity. It remains to define the advection velocity $\boldsymbol{c}$ in (21). In principle, it should be given by $\boldsymbol{c} = \boldsymbol{u} - \boldsymbol{u}^{\text{d}}$, as in (8), where $\boldsymbol{u}$ is the velocity field in the bulk of the flow and $\boldsymbol{u}^{\text{d}}$ the velocity of the domain due to the ALE formulation employed. However, very often (part of) the chlorination of the tank comes from little holes or hoses where water with a very high concentration of chlorine is injected. This process is often termed as rechlorination, as this is additional chlorine directly injected to the tank.

Let $\boldsymbol{u}_{\text{rec}}$, p_{rec} be the velocity and pressure associated to the flow induced by the rechlorination through the hoses. We assume that in most of the computational domain, $|\boldsymbol{u}_{\text{rec}}| \ll |\boldsymbol{u}|$ and therefore, *the bulk velocity is not influenced by* $\boldsymbol{u}_{rec}$. This is of course an approximation, which allows us to compute independently first $\boldsymbol{u}$ from (9) and (10) and then $\boldsymbol{u}_{\text{rec}}$.

We need to specify how to compute $\boldsymbol{u}_{\text{rec}}$. Because we assume that it is small, we neglect inertial effects in its calculation, as well as time variations. Let Γ_{rec} be the part of the boundary of the computational domain Ω where rechlorination takes place, which we assume is a submerged hole of $\partial\Omega$. We compute $\boldsymbol{u}_{\text{rec}}$, p_{rec} by solving the stationary Stokes problem:

$$\begin{aligned} -\nu\Delta\boldsymbol{u}_{\text{rec}} + \nabla p_{\text{rec}} &= \boldsymbol{0} && \text{in } \Omega \\ \nabla\cdot\boldsymbol{u}_{\text{rec}} &= 0 && \text{in } \Omega \\ \boldsymbol{u}_{\text{rec}} &= \bar{\boldsymbol{u}}_{\text{rec}} && \text{on } \Gamma_{\text{rec}} \\ \boldsymbol{u}_{\text{rec}} &= \boldsymbol{0} && \text{on } \partial\Omega \setminus \Gamma_{\text{rec}} \end{aligned}$$

where $\bar{\boldsymbol{u}}_{\text{rec}}$ is the velocity with which the chlorine is injected. Note that Ω is time dependent, and therefore, $\boldsymbol{u}_{\text{rec}}$ will change in time because of the change of the computational domain.

DOI: 10.1002/fld

Even if $\boldsymbol{u}_{\text{rec}}$ does not influence $\boldsymbol{u}$, it is obviously crucial in the transport of C, because part of this concentration comes from Γ_{rec}. Because $\boldsymbol{u}_{\text{rec}}$ is small, we assume that the flow it induces can be directly superimposed to the flow of $\boldsymbol{u}$. Thus, the advection velocity to be used in (21) is

$$\boldsymbol{c} = \boldsymbol{u} + \boldsymbol{u}_{\text{rec}} - \boldsymbol{u}^{\text{d}} \tag{23}$$

In Section 4, we will check numerically the validity of the approximation proposed.

2.3.2. Initial and boundary value problem. In view of the previous discussion, we can already write down the initial and boundary value problem for the chlorine concentration C.

Referring to the initial conditions, we can choose either prescribing C at $t = 0$ or prescribing periodical boundary conditions if a period of a long working operation of the tank is to be analyzed. The first condition is of the form $C(\boldsymbol{x}, t) = C^0(\boldsymbol{x})$, with $\boldsymbol{x}$ the spatial position and $C^0(\boldsymbol{x})$ a given function, whereas the latter would be of the form $C(\boldsymbol{x}, 0) = C(\boldsymbol{x}, T), \partial_t C(\boldsymbol{x}, 0) = \partial_t C(\boldsymbol{x}, T)$, assuming the initial time is set to $t = 0$ and T being now the period. To fix ideas, we will choose the first option, which is what we used in the numerical examples, with $C^0(\boldsymbol{x}) = 0$.

To write down the boundary conditions, let Γ_{in} the inflow part of the boundary, that is, the part of Γ_D where the velocity points to the interior of Ω (inlets and the jet on the free surface) and C_{in} the known chlorine concentration with which the flow enters the domain. On the rest of the boundary, we prescribe the no-flux condition $\boldsymbol{n} \cdot \nabla C = 0$.

Under all the assumptions described, the problem for the chlorine concentration consists of finding $C : \Omega \times [0, T] \longrightarrow \mathbb{R}$ such that

$$\begin{aligned}
\partial_t C + (\boldsymbol{u} + \boldsymbol{u}_{\text{rec}} - \boldsymbol{u}^{\text{d}}) \cdot \nabla C - \kappa_{\text{mol}} \Delta C + k\, C &= 0 && \text{in } \Omega,\ t \in (0, T) \\
C &= C_{\text{in}} && \text{in } \Gamma_{\text{in}},\ t \in (0, T) \\
C &= C_{\text{rec}} && \text{in } \Gamma_{\text{rec}},\ t \in (0, T) \\
\boldsymbol{n} \cdot \nabla C &= 0 && \text{in } \partial\Omega \setminus \Gamma_{\text{in}} \setminus \Gamma_{\text{rec}},\ t \in (0, T) \\
C &= 0 && \text{in } \Omega,\ t = 0
\end{aligned}$$

2.3.3. Variational problem. To model the evolution of the chlorine concentration C, we need to solve the boundary value problem for $\boldsymbol{u}_{\text{rec}}$ and then the initial and boundary value problem for C. In order to write the variational form of these problems, let us introduce the spaces:

$$\begin{aligned}
V_{\text{rec}} &:= \left\{ \boldsymbol{v} \in H^1(\Omega)^3 \mid \boldsymbol{v} = \boldsymbol{u}_{\text{rec}} \text{ on } \Gamma_{\text{rec}} \right\} \\
V_{\text{rec},0} &:= \left\{ \boldsymbol{v} \in H^1(\Omega)^3 \mid \boldsymbol{v} = \boldsymbol{0} \text{ on } \Gamma_{\text{rec}} \right\} \\
V_C &:= \left\{ D \in H^1(\Omega) \mid D = C_{\text{in}} \text{ on } \Gamma_{\text{in}},\ D = C_{\text{rec}} \text{ on } \Gamma_{\text{rec}} \right\} \\
V_{C,0} &:= \left\{ D \in H^1(\Omega) \mid D = 0 \text{ on } \Gamma_{\text{in}} \cup \Gamma_{\text{rec}} \right\}
\end{aligned}$$

The variational form of the problem for the rechlorination flow consists in finding $\boldsymbol{u}_{\text{rec}} \in V_{\text{rec}}$ and $p_{\text{rec}} \in L^2(\Omega)/\mathbb{R}$ such that

$$\nu(\nabla \boldsymbol{u}_{\text{rec}}, \nabla \boldsymbol{v}_{\text{rec}}) - (p_{\text{rec}}, \nabla \cdot \boldsymbol{v}_{\text{rec}}) + (q_{\text{rec}}, \nabla \cdot \boldsymbol{u}_{\text{rec}}) = 0 \tag{24}$$

for all $\boldsymbol{v}_{\text{rec}} \in V_{\text{rec},0}$ and $q_{\text{rec}} \in L^2(\Omega)/\mathbb{R}$, whereas the problem for the chlorine concentration in variational form consists in finding $C : [0, T] \longrightarrow V_C$ such that

$$(\partial_t C, D) + \langle (\boldsymbol{u} + \boldsymbol{u}_{\text{rec}} - \boldsymbol{u}^{\text{d}}) \cdot \nabla C, D \rangle + \kappa_{\text{mol}} (\nabla C, \nabla D) + k(C, D) = 0 \tag{25}$$

for all $D \in V_{C,0}$.

3. NUMERICAL APPROXIMATION

In this section, we present the numerical approximation of the various problems encountered and discuss some implementation issues. We use finite difference schemes for the time integration and finite element methods for the spatial approximation. The motivation for the numerical formulation we will describe can be found, for example, in [34–36, 50].

DOI: 10.1002/fld

3.1. Time discretization and time advancing algorithm

Let us consider a partition $0 = t^0 < t^1 < \ldots < t^N = T$ of the time interval into N time steps of size δt, taken constant for the sake of simplicity. The approximation of a time-dependent function f at time t^n will be denoted f^n. Likewise, the flow domain at time t^n will be denoted Ω^n.

Any time integration scheme can be used to approximate the evolution problems for the velocity and the chlorine concentration. For conciseness, let us assume that a backward difference formula of order r is used, so that $\delta_t^{(r)} f^n$ is the r-th order approximation to the time derivative at time t^n. In our examples, we use $r = 2$, that is to say,

$$\delta_t^{(2)} f^n = \frac{1}{2\delta t}\left(f^n - 4f^{n-1} + 3f^{n-2}\right)$$

The first order formula $\delta_t^{(1)} f^n = \delta t^{-1}(f^n - f^{n-1})$ needs to be used when $n = 1$.

Having introduced the time discretization, the sequential algorithm to solve the problem is the following:

- Set $\boldsymbol{u}^0 = \boldsymbol{0}, C^0 = 0$ or read the initial condition for $\boldsymbol{u}$ and C (time periodical boundary conditions are also allowed).
- For $n = 1, \ldots, N$ do the following:
  - Compute the domain velocity $\boldsymbol{u}^{\mathrm{d}}$ on Ω^{n-1} by solving (4)–(7) (very often the problem is trivial). Update the domain to Ω^n.
  - On Ω^n, solve for the velocity $\boldsymbol{u}^n$ and the pressure p^n from the time discrete version of (9) and (10), that is,

$$\left(\delta_t^{(r)}\boldsymbol{u}^n, \boldsymbol{v}\right) + \left\langle\left(\boldsymbol{u}^n - \boldsymbol{u}^{\mathrm{d}}\right)\cdot\nabla\boldsymbol{u}^n, \boldsymbol{v}\right\rangle + 2\nu\left(\nabla^s\boldsymbol{u}^n, \nabla^s\boldsymbol{v}\right) - \left(p^n, \nabla\cdot\boldsymbol{v}\right) = \langle\boldsymbol{f}, \boldsymbol{v}\rangle \tag{26}$$

$$\left(q, \nabla\cdot\boldsymbol{u}^n\right) = 0 \tag{27}$$

  - On Ω^n, solve the rechlorination problem (24) for $\boldsymbol{u}_{\mathrm{rec}}$ and p_{rec}, if needed.
  - On Ω^n, solve for the chorine concentration C^n from the time discrete version of (25), that is,

$$\left(\delta_t^{(r)}C^n, D\right) + \left\langle\left(\boldsymbol{u}^n + \boldsymbol{u}_{\mathrm{rec}} - \boldsymbol{u}^{\mathrm{d}}\right)\cdot\nabla C^n, D\right\rangle + \kappa_{\mathrm{mol}}(\nabla C^n, \nabla D) + k(C^n, D) = 0 \tag{28}$$

- End

3.2. Space discretization

Once the time discretization is performed, we need to discretize the problem in space. The spatial approximation of problems (4)–(7) is easy, and we shall not describe it here. When the solution is not a trivial scaling of the vertical coordinates, a simple Poisson solver needs to be used. Likewise, the finite element approximation of problem (24) is much simpler than that of the Navier–Stokes equations, of which it can be considered a particular case, so we will only describe our way to approximate (26)–(27), and also (28).

We assume that both problems are discretized using the same finite element mesh $\{K\}$, K denoting a generic element domain. We consider this mesh quasi-uniform, of size $h = \max\{h_K\}$, h_K being the diameter of element K. Summation over all elements will be indicated by $\sum_K$, and the L^2 product in K by $(\cdot,\cdot)_K$.

3.2.1. Navier–Stokes equations. The finite element approximation of problems (26) and (27) may suffer from two main sources of numerical instabilities, namely, the classical oscillations found in convection-dominated flows when the viscosity is small and the compatibility conditions between the velocity and pressure interpolation. In order to overcome both, we use a stabilized finite element method. Let $V_h \subset V$ and $Q_h \subset Q$ be the velocity and pressure finite element spaces, respectively, and $V_{0,h} \subset V_0$ the finite element space for the velocity test functions. We construct them with *equal* continuous interpolation. In particular, in the numerical simulations, we have taken linear tetrahedral elements.

DOI: 10.1002/fld

The approximation of problems (26) and (27) at each time step n consists of finding a velocity $\boldsymbol{u}_h^n \in V_h$ and a pressure $p_h^n \in Q_h$ such that

$$\begin{aligned}\left(\delta_t^{(r)}\boldsymbol{u}_h^n, \boldsymbol{v}_h\right) + \left\langle\left(\boldsymbol{u}_h^n - \boldsymbol{u}^{\mathrm{d}}\right)\cdot\nabla\boldsymbol{u}_h^n, \boldsymbol{v}_h\right\rangle + 2\nu\left(\nabla^s\boldsymbol{u}_h^n, \nabla^s\boldsymbol{v}_h\right)\\ - \left(p_h^n, \nabla\cdot\boldsymbol{v}_h\right) + \left(q_h, \nabla\cdot\boldsymbol{u}_h^n\right) + \mathcal{S}_{\mathrm{NS}}\left(\boldsymbol{u}_h - \boldsymbol{u}^{\mathrm{d}}; \boldsymbol{u}_h, p_h; \boldsymbol{v}_h, q_h; \boldsymbol{f}\right) = \langle\boldsymbol{f}, \boldsymbol{v}_h\rangle\end{aligned} \tag{29}$$

for all test functions $\boldsymbol{v}_h \in V_{0,h}$ and $q_h \in Q_h$, where the stabilizing term is given by

$$\begin{aligned}\mathcal{S}_{\mathrm{NS}}\left(\boldsymbol{c}; \boldsymbol{u}_h, p_h; \boldsymbol{v}_h, q_h; \boldsymbol{f}\right) &= \sum_K \tau_{u,K}(\boldsymbol{c})\left(-\mathcal{N}^*(\boldsymbol{c}; \boldsymbol{v}_h, q_h), P_h^{\perp}(\mathcal{N}(\boldsymbol{c}; \boldsymbol{u}_h, p_h) - \boldsymbol{f})\right)_K\\ \mathcal{N}^*(\boldsymbol{c}; \boldsymbol{v}_h, q_h) &= -\boldsymbol{c}\cdot\nabla\boldsymbol{v}_h - \nu\nabla\cdot\nabla^s\boldsymbol{v}_h - \nabla q_h\\ \mathcal{N}(\boldsymbol{c}; \boldsymbol{v}_h, q_h) &= \boldsymbol{c}\cdot\nabla\boldsymbol{v}_h - \nu\nabla\cdot\nabla^s\boldsymbol{v}_h + \nabla q_h\\ \tau_{u,K}(\boldsymbol{c}) &= \left(\frac{4\nu}{h_K^2} + \frac{2|\boldsymbol{c}|}{h_K}\right)^{-1}\end{aligned}$$

where $P_h^{\perp}$ is the projection orthogonal to the finite element space, that is to say, $P_h^{\perp}(f) = f - P_h(f)$, P_h being the L^2 projection onto V_h. We usually lag this projection either one iteration or one-time step. In the latter case for example, we would have $P_h^{\perp}(f^n) \approx f^n - P_h(f^{n-1})$. Refer to [35, 36] for further details.

Apart from a more or less standard iterative procedure to deal with the different nonlinearities, the basic numerical formulation presented earlier has been implemented using some features, which will not be detailed here. These are the following:

- Nodal-based implementation [34]. This implementation is based on an *a priori* calculation of the integrals appearing in the formulation and then the construction of the matrix and right-hand-side vector of the final algebraic system to be solved. After appropriate approximations, this matrix and this vector can be constructed directly for each nodal point, without the need to loop over the elements and thus making the calculations much faster. In order to be able to do this, all the variables have to be defined at the nodes of the finite element mesh, not on the elements. This is also so for the stabilization parameters of the formulation.
- Predictor–corrector scheme [36]. The pressure segregation is inspired in fractional step schemes, although the converged solution corresponds to that of a monolithic time integration.

The reader is referred to the references indicated in each item for details.

An important feature of our formulation is that we do not introduce any turbulence model and rely on the dissipative structure of the numerical model to simulate the effect of the unresolved scales. This approach is known as implicit large eddy simulation. A full discussion on the theoretical basis of this strategy can be found in [49], and a thorough assessment of its performance in classical turbulence benchmark problems in [51].

3.2.2. Chlorine concentration equation. Let us consider now the finite element approximation of (28). Again, we construct the finite element space for C^n using continuous interpolations, the same as for the velocity and the pressure in the Navier–Stokes equations. Let $V_{C,h} \subset V_C$ be the resulting finite element space and $V_{C,0,h}$ the corresponding space of test functions. The approximation we use at each time step consists in finding $C_h^n \in V_{C,h}$ such that

$$\begin{aligned}\left(\delta_t^{(r)}C_h^n, D_h\right) + \left\langle\left(\boldsymbol{u}_h^n + \boldsymbol{u}_{\mathrm{rec},h} - \boldsymbol{u}^{\mathrm{d}}\right)\cdot\nabla C_h^n, D_h\right\rangle + \kappa_{\mathrm{mol}}\left(\nabla C_h^n, \nabla D_h\right) + k\left(C_h^n, D_h\right)\\ + \mathcal{S}_{\mathrm{C}}\left(\boldsymbol{u}_h + \boldsymbol{u}_{\mathrm{rec},h} - \boldsymbol{u}^{\mathrm{d}}; C_h^n, D_h\right) + \mathcal{D}_{\mathrm{C}}\left(\boldsymbol{u}_h + \boldsymbol{u}_{\mathrm{rec},h} - \boldsymbol{u}^{\mathrm{d}}; C_h^n, D_h\right) = 0\end{aligned} \tag{30}$$

DOI: 10.1002/fld

for all $D_h \in V_{C,0,h}$, where $\boldsymbol{u}_{\mathrm{rec},h}$ is a finite element approximation of $\boldsymbol{u}_{\mathrm{rec}}$. It is observed from (30) that two terms have been added to the standard Galerkin terms. The first is in charge of stabilizing convection-dominated flows and is similar to the one encountered for the Navier–Stokes equations. It is given by

$$\begin{aligned}
\mathcal{S}_{\mathrm{C}}(\boldsymbol{c}; C_h, D_h) &= \sum_K \tau_{C,K}(\boldsymbol{c})(-\mathcal{C}^*(\boldsymbol{c}; C_h), P_h^{\perp}(\mathcal{C}(\boldsymbol{c}; D_h))_K \\
\mathcal{C}^*(\boldsymbol{c}; D_h) &= -\boldsymbol{c}\cdot\nabla D_h - \kappa_{\mathrm{mol}}\Delta D_h + rD_h \\
\mathcal{C}(\boldsymbol{c}; D_h) &= \boldsymbol{c}\cdot\nabla D_h - \kappa_{\mathrm{mol}}\Delta D_h + rD_h \\
\tau_{C,K}(\boldsymbol{c}) &= \left(\frac{4\kappa_{\mathrm{mol}}}{h_K^2} + \frac{2|\boldsymbol{c}|}{h_K}\right)^{-1}
\end{aligned}$$

where $P_h^{\perp}$ stands now for the orthogonal projection onto $V_{C,h}$.

With the introduction of $\mathcal{S}_{\mathrm{C}}\left(\boldsymbol{u}_h + \boldsymbol{u}_{\mathrm{rec},h} - \boldsymbol{u}^{\mathrm{d}}; C_h^n, D_h\right)$, it is possible to obtain globally stable solutions in convection-dominated flows, that is to say, flows with small κ_{mol}. However, small oscillations localized near sharp gradients of the solution may still remain. In the problem we are considering, these regions appear in the jets of chlorine injected into the tank. The chlorine concentration in these jets is higher than that of the water in the tank, and very sharp gradients appear close to the entrance of the jets. In fact, the chlorine concentration is discontinuous on the boundary of the tank.

The term $\mathcal{D}_{\mathrm{C}}\left(\boldsymbol{u}_h + \boldsymbol{u}_{\mathrm{rec},h} - \boldsymbol{u}^{\mathrm{d}}; C_h^n, D_h\right)$ in (30) is designed to avoid localized oscillations. It is what is often called a *discontinuity capturing* or shock capturing term. In the modeling of water tanks, we have found very effective to compute it as it is explained in [50], where it is proposed but not tested:

$$\begin{aligned}
\mathcal{D}_{\mathrm{C}}\left(\boldsymbol{c}; C_h^n, D_h\right) &= \sum_K \kappa_{K,\mathrm{dc}}(\boldsymbol{c}, C_h)(\nabla C_h, \nabla D_h) \\
\kappa_{K,\mathrm{dc}}(\boldsymbol{c}, C_h) &= \frac{1}{2}\alpha\left(\kappa_{\mathrm{mol}} + |\boldsymbol{c}|h_K + rh_K^2\right)\frac{|P_h^{\perp}(\nabla C_h)|}{|\nabla C_h|} \\
\alpha &= \max\{0, 1 - |\boldsymbol{c}|h_K/(2\kappa_{\mathrm{mol}})\}
\end{aligned}$$

Note that $\kappa_{K,\mathrm{dc}}(\boldsymbol{c}, C_h)$ is a nonlinear diffusion that acts only when the Péclet number of the chlorine concentration equation is high and when $\left|P_h^{\perp}(\nabla C_h)\right|$ is high compared with $|\nabla C_h|$, which can be understood as a situation in which the finite element mesh is not able to capture gradients of finite element functions.

In Section 4, we will present (for the first time) a simple example showing the usefulness of introducing this discontinuity capturing term, in particular in the entrance of jets in a water tank. Apart from solving a simple problem to better understand its effect, we have also applied it in the simulation of real water tanks.

4. NUMERICAL SIMULATIONS

In this section, we present some numerical simulations obtained using the numerical formulation developed in this paper. We start with a section testing some of the new numerical ingredients proposed, in particular the shock-capturing technique, the approximation of the jet boundary conditions, and the approximation of small jets into a bulk flow. The tailored ALE formulation proposed is directly tested in the next application cases.

As application examples, we present the results of the numerical simulation of two water storage tanks. These results are very qualitative, with the only intention to demonstrate the potential of the model we have developed to determine the time evolution of the chlorine concentration.

The mathematical and numerical model has been fully described, including the value of the physical constants and the numerical parameters used in the calculations. In the two cases analyzed, the simulation time has been $T = 24$ h, and zero initial conditions have been assumed, both for velocity

DOI: 10.1002/fld

and for chlorine concentration. The time step has being taken as $\delta t = 1$ s, and therefore, 86,400 time steps have been computed in both problems. From the modeling point of view, it only remains to describe the setting of the problem and, from the numerical side, the mesh used.

4.1. Testing some of the new ingredients of the formulation

In this subsection, we present some simple tests to quantify some of the novel modeling or numerical approximations proposed in this paper, in particular

- The way to treat the advection velocity in the chlorine concentration equation (explained in Subsection 2.3.1). In essence, we propose to superpose the flow of the small chlorine jet to the bulk flow (which is obviously an approximation for nonlinear flow problems).
- The need for a discontinuity capturing term in the approximation of the chlorine concentration equation (explained in Subsection 3.2.2). Results using this method are here presented for the first time.
- The model for the falling of water jets (explained in Subsection 2.2.2), and in particular the comparison between options (19) and (20).

4.1.1. Comparison of exact and approximated advection velocities in the chlorine concentration equation. In this numerical example we compare the final chlorine concentration results using an exact treatment of the chlorine injection (doing the whole simulation of all inflow conditions in a single step) and the approximated one (taking into account independently $\boldsymbol{u}_h$ and $\boldsymbol{u}_{\mathrm{rec},h}$, the approximation to $\boldsymbol{u}_{\mathrm{rec}}$). The following bidimensional problem is considered: the computational domain consists of a rectangle of dimensions $10 \times 2\mathrm{m}^2$. A 0.02-m wide injection jet with an inflow velocity of 0.01 m/s is entering through the left wall between y-coordinates 0.99 m and 1.01 m, the chlorine concentration being 0.001 kg/m^3. A 0.4-m wide, chlorine-free water jet is impacting the upper boundary with an inflow velocity of 0.5 m/s in the area between x-coordinates 4.8 and 5.2. In the rest of the upper boundary, an outflow velocity is set so that the incompressibility constraint is fulfilled in the whole computational domain.

Figure 5 shows a comparison of the results after 500 s of the chlorination process has been simulated, considering both the whole advection velocity $\boldsymbol{c} = \boldsymbol{u}_h + \boldsymbol{u}_{\mathrm{rec},h}$ in a single simulation, or, on the contrary, solving independently for $\boldsymbol{u}_h$ using the Navier–Stokes equations and for $\boldsymbol{u}_{\mathrm{rec},h}$ using a stationary Stokes problem. In can be seen that results for both velocity and chlorine concentration are very similar, from which we conclude that the approximation introduced does not significantly affect the accuracy of the method for the small chlorine injection velocities that have to be considered in practice.

4.1.2. Testing the shock capturing method. In this numerical example, we test the efficiency of the shock capturing technique for eliminating the local numerical oscillations, which appear in the areas with large concentration gradients. The computational domain is again a rectangle of dimensions $10 \times 2\mathrm{m}^2$. A 0.02-m wide injection jet with an inflow velocity of 0.01 m/s is entering through the left wall between y-coordinates 0.49 and 0.51 m, the chlorine concentration being 0.001 kg/m^3. No

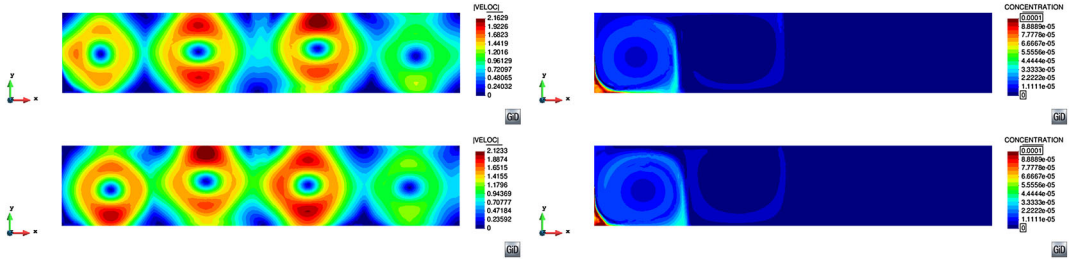

Figure 5. Comparison of results for different methods to compute the advection velocity. Top: monolithic approach; bottom: partitioned approach; left: velocity norm contours; and right: concentration contours.

DOI: 10.1002/fld

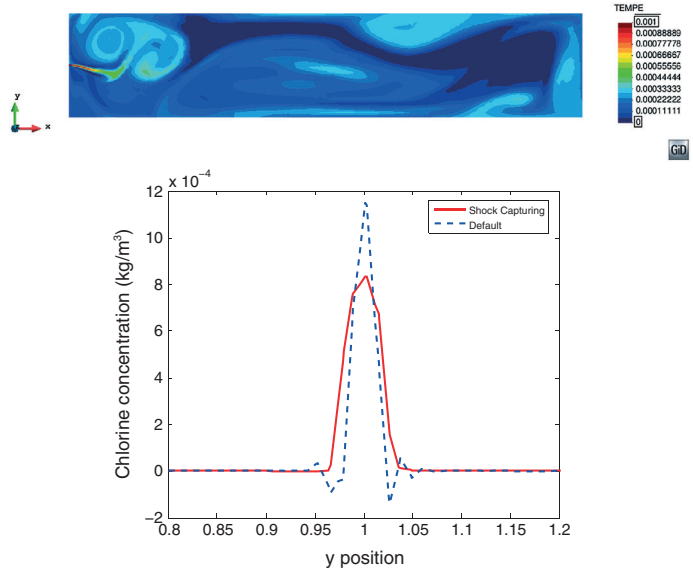

Figure 6. Results for the chlorinated jet injection after 20,000 s of simulation. Top: chlorine concentration field and bottom: chlorine concentration at a cut along $x = 0.1$ m.

water jet in the superior boundary is considered, and an appropriate exit velocity is set in the top boundary so that the incompressibility constraint is fulfilled. Figure 6 shows a comparison of the results with and without shock capturing. The results without the shock capturing terms show spurious numerical oscillations in the area surrounding the jet injection. These oscillations are completely dumped with the shock capturing technique.

4.1.3. Water jet entry profile. In this section, we test the numerical performance of the approximation for the water jet entry profile, that is, we compare the results obtained with (19) and (20). In order to do this, a restriction to the bidimensional case of the water jet entry profile is considered. The first step consists in imposing the momentum conservation in the bidimensional case. Similar to the three-dimensional case, we first need to enforce the continuity equation:

$$2\rho U_0 R_0 = 2M(0,L)\int_0^R \left[1-\left(\frac{r}{R}\right)^{3/2}\right]^3 \mathrm{d}\,r$$

from which we obtain the 2D-counterpart of (14)

$$M(0,L) = 2.71\rho U_0 \frac{R_0}{R}$$

from where we get

$$U(r,L) = 2.71\,U_0 \frac{R_0}{\alpha R}\left[1-\left(\frac{r}{R}\right)^{3/2}\right]^3$$

Because only the α fraction of the jet is composed of water, the water entry velocity to consider in the numerical simulation will be

$$U(r,L) = 2.71 U_0 \frac{R_0}{R}\left[1-\left(\frac{r}{R}\right)^{3/2}\right]^3$$

In this numerical example, a 0.2-m diameter jet ($R_0 = 0.1$ m) with an inflow velocity $U_0 = 1$ m/s at a height of the center of $Z_0 = 1$ m is going to be considered. The water surface impact time of the center of the jet is $T_\mathrm{f} = \sqrt{2Z_0/g} = 0.4515$ s. The impact velocity considering only

DOI: 10.1002/fld

uniform horizontal movement and accelerated vertical movement is $\boldsymbol{u} = (1, -4.42)$ m/s, and the horizontal distance traveled by the water jet is $L = 0.4515$ m. This allows us to compute the direction of the jet at the impact point: $\hat{\boldsymbol{u}} = (0.22, -0.975)$. The jet radius at the impact point is $R = R_0 + 0.005L = 0.1023$ m. The impact velocity profile to be considered along an impact region of radius $R = 0.1023$ m is the following:

$$\boldsymbol{u}^{\text{jet}} = 2.7723 \left[1 - \left(\frac{r}{0.1023} \right)^{3/2} \right]^3 \hat{\boldsymbol{u}} \text{ m/s} \tag{31}$$

which is the 2D-counterpart of (19). This is going to be compared with the result of applying the simplified velocity profile given (20), which in this case reduces to

$$\boldsymbol{u}^{\text{jet}} = \hat{\boldsymbol{u}} \text{ m/s} \tag{32}$$

Figure 7 shows a comparison of the profiles of both (modeled and approximated) inflow velocities.

Moreover, the impact-projected surface radius in the streamline direction can be computed as

$$r_{\text{impact}} = \frac{r}{\cos(\theta)}, \quad 0 \leqslant r \leqslant R$$

where θ is the angle of $\hat{\boldsymbol{u}}$ with respect to the vertical direction. For this numerical example, $\cos(\theta) = 0.975$.

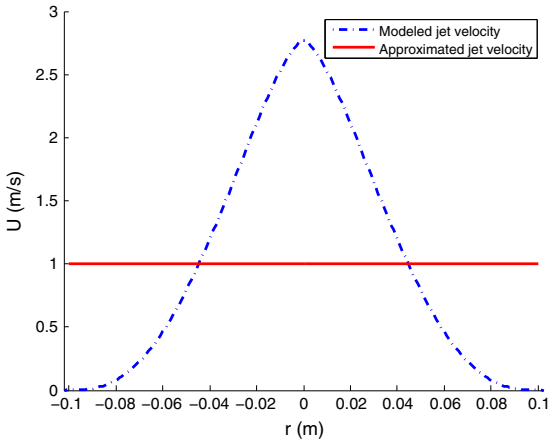

Figure 7. Comparison of modeled and approximated jet velocity profiles.

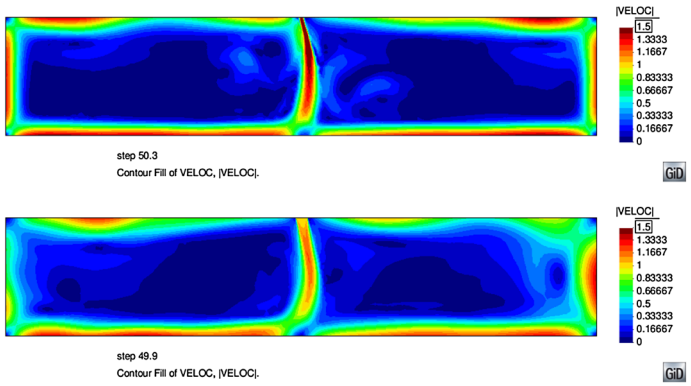

Figure 8. Comparison of velocity fields after 50 s of simulation for the modeled (top) and approximated (bottom) jets.

DOI: 10.1002/fld

The computational domain in this example is again a 10×2 m^2 tank, in this case with the jet impacting in the middle of the upper boundary of the tank. An appropriate outflow velocity is set in the rest of the water surface so that the incompressibility constraint is fulfilled. Figure 8 shows the comparison of the velocity norms obtained using (31) and (32). The physical and geometrical parameters employed are of the order of those encountered in practical applications. It is observed that the resulting flow patterns are similar, particularly considering all the approximations (physical and numerical) of the model.

4.2. Water tank 1

In this first application example, we show the results corresponding to the numerical simulation of the water tank shown in Figure 9. The left side of this picture shows where the water inlet is located. In this case, there is a jet of water (E) that impacts the time-dependent free surface, where the model

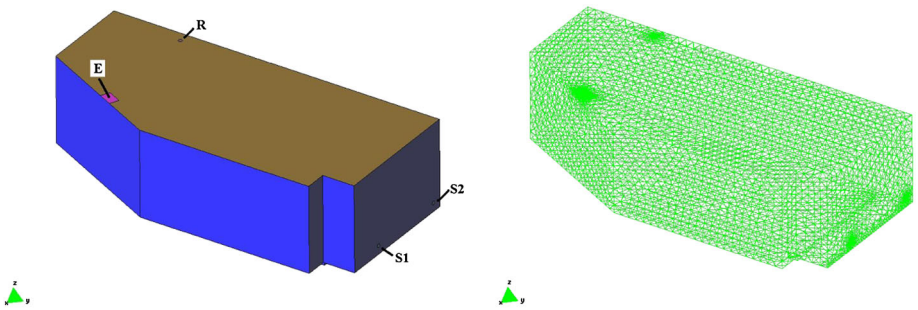

Figure 9. Water tank 1. Left: geometry, showing inlet (E), outlets (S1, S2), and rechlorination inlet (R). Right: finite element mesh of 111,788 tetrahedral elements.

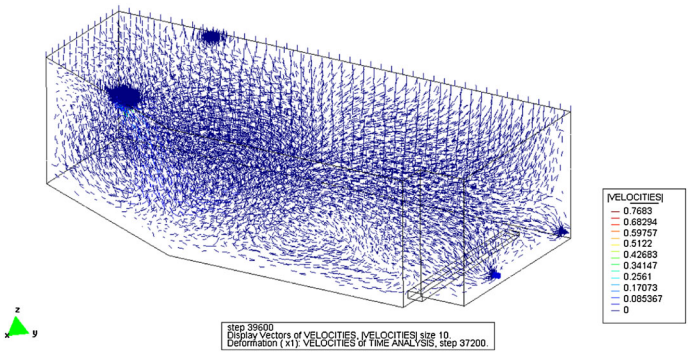

Figure 10. Water tank 1. Velocity vectors at $t = 10,000$ s.

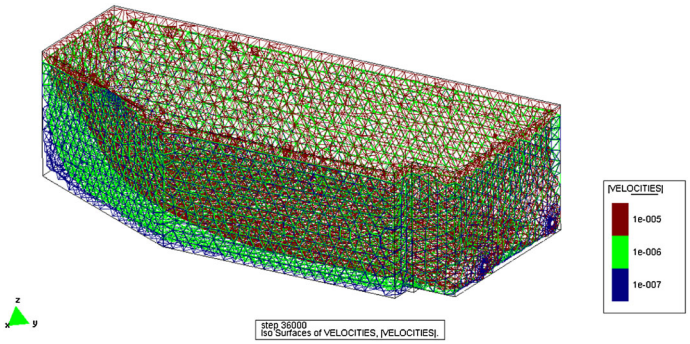

Figure 11. Water tank 1. Contours of the norm of velocity vectors at $t = 10,000$ s.

DOI: 10.1002/fld

described in Section 2 has been used. In this case, there are two outlets, S1 and S2. A flow rate is prescribed in the former, whereas the latter is left free. Finally, chlorine is introduced in this example through a little hole placed close to the top of the tank wall (R).

The finite element mesh used in this example is shown in the right picture of Figure 9. It is a relatively coarse mesh made of 111,788 linear tetrahedral elements. Nevertheless, the stabilized finite element method described in Section 3 is able to capture the large scales of the flow and provide a stable numerical simulation. It is observed that the finite element mesh has been refined in the regions close to the inlets and outlets.

Velocity vectors at $t = 10,000$ s are shown in Figure 10. The interest of having a global picture of the velocity field is that dead zones can be easily identified. These zones are potential areas of problems, either because chlorine takes a long time to arrive there (by diffusive mechanisms) or because water particles have a long residence time, allowing for its deterioration. Additional information can be obtained looking at the contours of the norm of the velocity field, which are shown in Figure 11 for a well-advanced simulation time.

Perhaps, the most relevant quantity to be computed is the concentration of chlorine at all points of the computational domain and all time instants. Different iso-surfaces of chlorine concentration at $t = 10,000$ s are shown in Figure 12. The reference concentration at the chlorination inlet (R) is 1 (note that the equation for C is linear).

This simulation has been performed according to the demand–supply curves shown in Figure 13. In fact, in this case, two demand curves have been considered, leading to two different simulations. With these curves, it is possible to determine the evolution of the free surface in time, apart of course of fixing the boundary conditions.

A simple outcome of the simulation that can be easily monitored is the chlorine concentration at the outlet. This is shown in Figure 13 (right picture) for the two simulations considered. Note that it takes some time until chlorine arrives to the exit, and then it grows until the end of the simulation time. If several days were simulated, a permanent regime would be obtained.

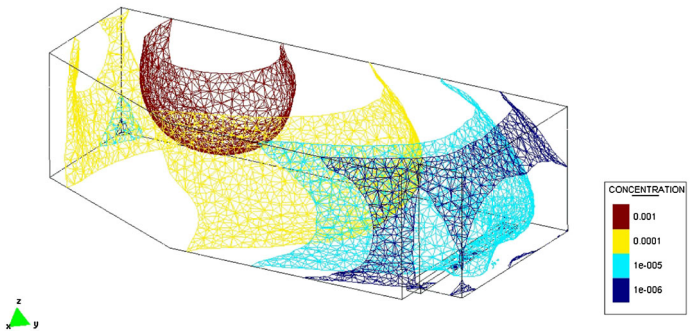

Figure 12. Water tank 1. Different iso-surfaces of chlorine concentration at $t = 10,000$ s.

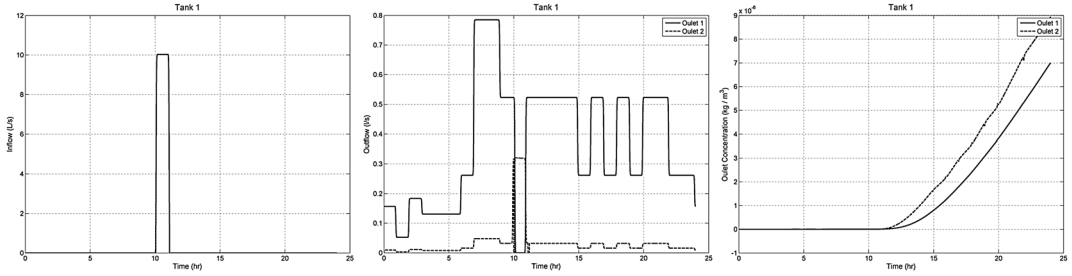

Figure 13. Water tank 1. Left: Supply curve. Middle: Demand curve for two different simulations. Right: Chorine concentration at the outlet in time for the two different simulations.

DOI: 10.1002/fld

4.3. Water tank 2

In this second application example, we perform a simulation similar to the previous one but with a different setting. In this case, the water tank is cylindrical, with several columns that support a lid that covers it. The geometry is shown in Figure 14, where the rechlorination inlet (R), the water inlet (E), and the outlet (S) can be observed. In this case, the jet of the inlet is always below the free surface, and therefore, it is only necessary to fix the inlet velocity as boundary condition.

The finite element mesh used in this example is shown in the right picture of Figure 14. Once again, it is a relatively coarse mesh made of 113,951 linear tetrahedral elements, but the large scales of the flow can be captured with the formulation we have used.

To visualize the dynamics of the flow in the region close to the inlet and the outlet, the trajectories of a few particles are shown in Figure 15. These trajectories are chosen as those with a short length from the inlet to the outlet. Other particles flow over all the tank in a much more complex pattern.

Contours of velocity norm at two different time instants are shown in Figure 16. As mentioned earlier, this information may serve to localize dead flow zones in the tank. The other important output of the simulation, namely, the iso-surfaces of chlorine concentration, are shown in Figure 17 at $t = 10,000$ s.

This simulation has been performed according to the demand–supply curves shown in Figure 18, with which it is possible to determine the evolution of the free surface in time, apart of fixing the boundary conditions. In the right picture of Figure 18 the evolution of C in time at a point in the outlet is observed. After an initial transient, this concentration oscillates around a mean value.

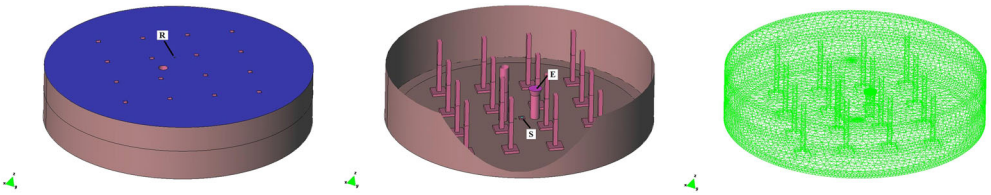

Figure 14. Water tank 2. Left: geometry of the boundary of the tank, showing the rechlorination inlet (R); middle: geometry of the interior of the tank, showing the inlet (E) and the outlet (S); and right: finite element mesh of 113,951 tetrahedral elements.

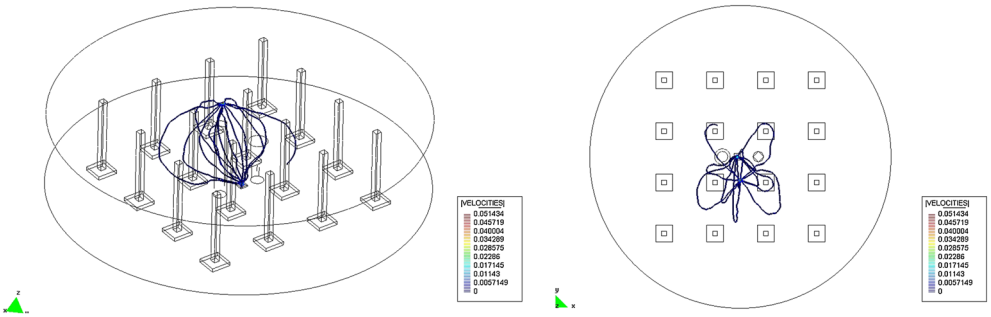

Figure 15. Water tank 2. Two views of particle tracking in the region close to the inlet.

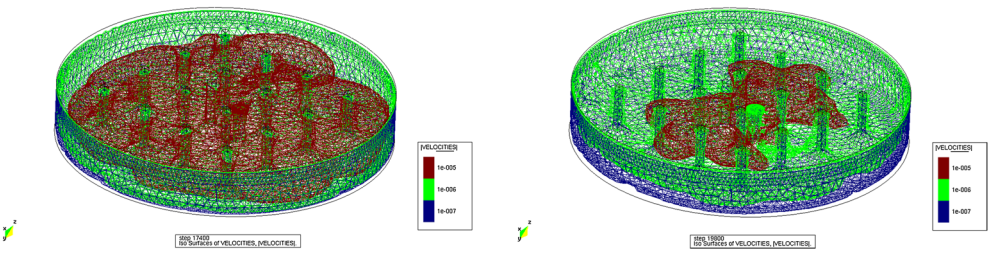

Figure 16. Water tank 2. Iso-velocity contours at two time instants.

DOI: 10.1002/fld

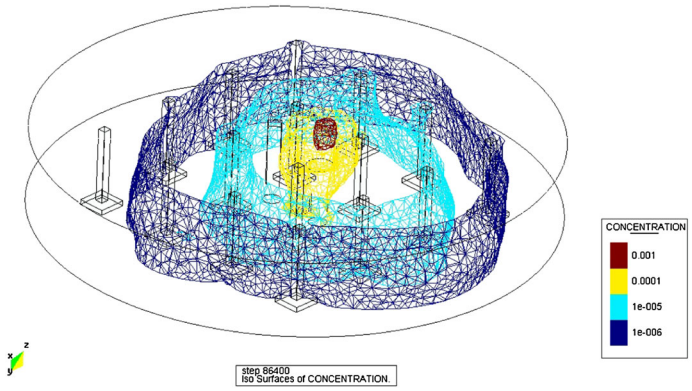

Figure 17. Water tank 2. Iso-surfaces of chlorine concentration at $t = 10,000$ s.

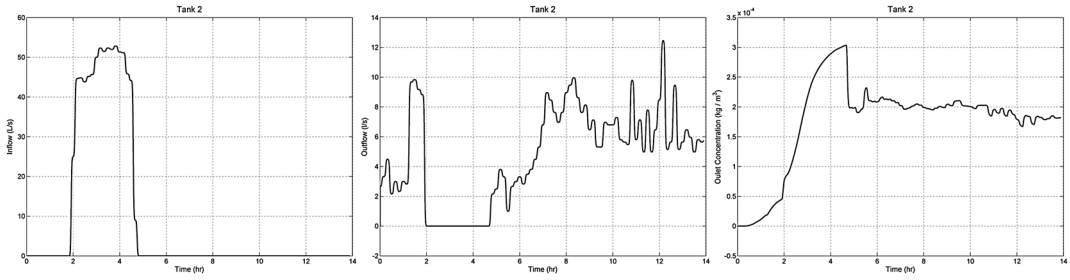

Figure 18. Water tank 2. Left: supply curve, middle: demand curve, and right: chorine concentration at the outlet in time.

5. CONCLUSIONS

In this paper, we have presented a *complete model* to simulate the hydrodynamics and evolution of chlorine concentration in water tanks. This model has different *original ingredients*, both from the physical and from the numerical modeling sides. From the physical viewpoint, apart from setting the standard equations for the flow problem and for the concentration of chlorine, we have proposed *strategies to treat the water jets* that feed the tank, the *motion of the free surface from the demand–supply curves*, or the *injection of chlorine through inlets of small diameter.* From the numerical side, we have presented *the finite element formulation we use*, which includes stabilization terms to allow equal interpolation of all variables and convection-dominated flows, as well as a *discontinuity capturing method* to cope with very high gradients of the solution, tested here for the first time.

The physical model proposed allows us to simulate the physical phenomenon with all its features and with what we believe are reasonable approximations. The numerical formulation has demonstrated its robustness, yielding numerical approximations free of oscillations and physically reliable. We believe that the complete model has a great potential to optimize water chorination in tanks, including if necessary more sophisticated models than those used here.

ACKNOWLEDGEMENTS

The model presented in this paper was developed in the context of the project QUALITAX, promoted and leadered by the Centre Tecnològic de l'Aigua (CETAQUA), in Barcelona, Spain. This support is gratefully acknowledged. R. Codina also acknowledges the support received from the ICREA Acadèmia Program, from the Catalan Government, and C. Muñoz acknowledges the support of a CONICYT doctoral scholarship from the Chilean Government.

DOI: 10.1002/fld

REFERENCES

1. van der Walt JJ. The modelling of water treatment process tanks. *Ph.D. Thesis*, Rand Afrikaans University, 2004.
2. Rossman LA, Uber JG, Grayman WM. Modeling disinfectant residuals in drinking-water storage tanks. *Journal of Environmental Engineering* 1995; **121**(10):752–755.
3. Levenspiel O. *Chemical Reaction Engineering* (3rd edition). Wiley, 1998.
4. Kohpaeia AJ, Sathasivan A. Chlorine decay prediction in bulk water using the parallel second order model: an analytical solution development. *Chemical Engineering Journal* 2011; **171**(1):232–241.
5. Clark RM. Chlorine demand and trihalomethane formation kinetics: a second-order model. *Journal of Environmental Engineering* 1998; **124**(1):16–24.
6. EPA. Comprehensive surface water treatment rules quick reference guide: unfiltered systems, 2004. Online, EPA 816-F-04-001.
7. Yeung H. Modelling of service reservoirs. *Journal of Hydroinformatics* 2001; **3**(3):165–172.
8. Mau RE, Boulos PF, Bowcock RW. Modelling distribution storage water quality: an analytical approach. *Applied Mathematical Modelling* 1996; **20**:329–338.
9. Roberts PJW, Tian X, Lee S, Sotiropoulos F, Duer M. Mixing in water storage tanks. *Technical Report E20-J08*, AWWA Research Foundation, 2005.
10. Bateman A, Medina V, Mujal A. Experimental study on mixing efficiency in water supply rectangular tanks. *EGU General Assembly*, Vol. 11, Vienna, Austria, 2009.
11. Greene DJ, Hass CN, Farouk B. Computational fluid dynamics analysis of the effects of reactor configuration on desinfection efficiency. *Water Environment Research* 2006; **78**:909–919.
12. Powell JC, West JR, Hallam NB, Forster CF, Simms J. Performance of various kinetic models for chlorine decay. *Journal of Water Resources Planning and Management* 2000; **126**(1):13–20.
13. Hua F, West JR, Barker RA, Forster CF. Modelling of chlorine decay in municipal water supplies. *Water Research* 1999; **33**(12):2735–2746.
14. Clark RM, Sivaganesan M. Predicting chlorine residuals in drinking water: second order model. *Journal of Water Resources Planning and Management* 2002; **128**(2):152–161.
15. Gang DC, Clevenger TE, Banerji SK. Modeling chlorine decay in surface water. *Journal of Environmental Informatics* 2003; **1**(1):21–27.
16. Shiono K, Teixeira EC. Turbulent characteristics in a baffled contact tank. *Journal of Hydraulic Research* 2000; **38**(6):403–416.
17. Yu X, Mazurek A, Putz G, Albers C. Physical and computational modelling of residence and flow development time in a large municipal desinfection clearwell. *Canadian Journal of Civil Engineering* 2010; **37**:931–940.
18. Wang H, Falconer RA. Numerical modeling of flow in chlorine disinfection tanks. *Journal of Hydraulic Engineering* 1998; **124**(9):918–931.
19. Amini R, Taghipour R, Mirgolbabaei H. Numerical assessment of hydrodynamic characteristics in chlorine contact tank. *International Journal for Numerical Methods in Fluids* 2011; **67**(7):885–898.
20. Kim D, Kim DI, Kim JH, Stoesser T. Large eddy simulation of flow and tracer transport in multichamber ozone contactors. *Journal of Environmental Engineering* 2010; **136**(1):22–31.
21. Hannoun IA, Boulos PF. Optimizing distribution storage water quality: a hydrodynamics approach. *Applied Mathematical Modelling* 1997; **21**:495–502.
22. Kleine D, Reddy BD. Finite element analysis of flows in secondary settling tanks. *International Journal for Numerical Methods in Engineering* 2005; **64**(7):849–876.
23. Vellando P, Puertas J, Colominas I. SUPG stabilized finite element resolution of the Navier–Stokes equations: applications to water treatment engineering. *Computer Methods in Applied Mechanics and Engineering* 2002; **191**(51–52):5899–5922.
24. Webb SW, van Bloemen BG. High fidelity computational fluid dynamics for mixing in water distribution systems. *8th Annual Water Distribution Systems Analysis Symposium*, Cincinnati, Ohio, USA, 2006t.
25. Santoro D, Bartrand TA, Greene DJ, Farouk B, Haas CN, Notarnicola M, Liberti L. Use of CFD for wastewater disinfection process analysis: E.coli inactivation with Peroxyacetic Acid (PAA). *International Journal of Chemical Reactor Engineering* 2005; **3**(A46).
26. Marek M, Stoesser T, Roberts PJW, Weitbrecht V, Jirka GH. CFD modeling of turbulent jet mixing in a water storage tank. *32nd IAHR Congress*, Venice, Italy, 2007.
27. Martinez-Solano F, Iglesias P, Gualtieri C, Lopez-Jimenez P. Modelling flow and concentration field in rectangular water tanks. *International Congress on Environmental Modelling and Software*, Ottawa, Ontario, Canada, 2010.
28. Brown L, Jacobsen F. Optimise tank design using CFD. *72nd Annual Victorian Water Industry Engineers and Operators Conference*, Bendigo, Victoria, Australia, 2009; 89–95.
29. Rossman LA, Grayman WM. Scale-model studies of mixing in drinking water storage tanks. *Journal of Environmental Engineering* 1999; **125**(8):755–761.
30. Wang H, Falconer RA. Simulating disinfection processes in chlorine contact tanks using various turbulence models and high-order accurate diference schemes. *Water Research* 1998; **32**(5):1529–1543.
31. Donea J, Huerta A, Ponthot JP, Rodriguez-Ferran A. Arbitrary Lagrangian–Eulerian methods. In *Encyclopedia of computational mechanics, Vol.1: Fundamentals*, Stein E, de Borst R, Hughes TJR (eds). John Wiley & Sons, 2004; 413–437.

DOI: 10.1002/fld

32. Boersma BJ, Brethouwer G, Nieuwstadt FTM. A numerical investigation on the effect of the inflow conditions on the self-similar region of a round jet. *Physics of Fluids* 1998; **10**(4):899–909.
33. Xu G, Antonia RA. Effect of different initial conditions on a turbulent round free jet. *Experiments in Fluids* 2002; **33**:677–683.
34. Codina R. A nodal-based implementation of a stabilized finite element method for incompressible flow problems. *International Journal for Numerical Methods in Fluids* 2000; **33**:737–766.
35. Codina R. Stabilized finite element approximation of transient incompressible flows using orthogonal subscales. *Computer Methods in Applied Mechanics and Engineering* 2002; **191**:4295–4321.
36. Codina R, Folch A. A stabilized finite element predictor–corrector scheme for the incompressible Navier–Stokes equations using a nodal based implementation. *International Journal for Numerical Methods in Fluids* 2004; **44**: 483–503.
37. Teixeira EC, Siqueira RN. Performance assessment of hydraulic efficiency indexes. *Journal of Environmental Engineering* 2008; **134**(10):851–859.
38. Madeira LM, Alves MA, Rodrigues AE. Teaching nonideal reactors with CFD tools. *Chemical Engineering Education* 2004; **38**:154–160.
39. Soulaimani A, Saad Y. An arbitrary Lagrangian–Eulerian finite element method for solving three-dimensional free surface flows. *Computer Methods in Applied Mechanics and Engineering* 1998; **162**:79–106.
40. Evans GM, Rielly CD. Free jet expansion and gas entrainment characteristics of a pluging liquid jet. *Experimental Thermal and Fluid Science* 1996; **12**:142–149.
41. Lin SP, Reitz RD. Drop and spray formation from a liquid jet. *Annual Review of Fluid Mechanics* 1998; **30**:85–105.
42. Sallam KA, Dai Z, Faeth GM. Liquid breakup at the surface of turbulent round liquid jets in still gases. *International Journal of Multiphase Flow* 2002; **28**(3):427–449.
43. Yoon SS, Hewson JC, DesJardin PE, Glaze DJ, Black AR, Skaggs RR. Numerical modeling and experimental measurements of a high speed solid-cone water spray for use in fire suppression applications. *International Journal of Multiphase Flow* 2004; **30**(11):1369–1388.
44. Guha A, Barron RM, Balachandar R. An experimental and numerical study of water jet cleaning process. *Journal of Materials Processing Technology* 2011; **211**(4):610–618.
45. Guha A, Barron RM, Balachandar R. Numerical simulation of high-speed turbulent water jets in air. *Journal of Hydraulic Research* 2010; **48**(1):119–124.
46. Rajaratnam N, Rizvi SSH, Steffler PM, Smy PR. An experimental study of very high velocity circular water jets in air. *Journal of Hydraulic Research* 1994; **32**(3):461–470.
47. Rajaratnam N, Albers C. Water distribution in very high velocity water jets in air. *Journal of Hydraulic Engineering* 1998; **124**(6):647–650.
48. Principe J, Codina R, Henke F. The dissipative structure of variational multiscale methods for incompressible flows. *Computer Methods in Applied Mechanics and Engineering* 2010; **199**:791–801.
49. Guasch O, Codina R. Statistical behavior of the orthogonal subgrid scale stabilization terms in the finite element large eddy simulation of turbulent flows. *Computer Methods in Applied Mechanics and Engineering* 2013; **261-262**: 154–166.
50. Codina R. Finite element approximation of the convection–diffusion equation: subgrid-scale spaces, local instabilities and anisotropic space-time discretizations. In *Bail 2010 - Boundary and Interior Layers, Computational and Asymptotic Methods*, vol. 81, Clavero C, Gracia JL, Lisbona FJ (eds)., Lecture Notes in Computational Science and Engineering. Springer, 2011; 85–97.
51. Colomés O, Badia S, Codina R, Principe J. Assessment of variational multiscale models for the large eddy simulation of turbulent incompressible flows. *Computer Methods in Applied Mechanics and Engineering* 2015; **285**:32–63.

DOI: 10.1002/fld